Aeroelastic Stability for Straight and Swept-Tip Rotor Blades in Hover and Forward Flight

Thomas H. Maier and David L. Sharpe
Army/NASA Rotorcraft Division
Aeroflightdynamics Directorate (AVRDEC)
US Army Aviation and Missile Command
Ames Research Center, Moffett Field, California

Anita I. Abrego
Army/NASA Rotorcraft Division
National Aeronautics and Space Administration
Ames Research Center, Moffett Field, California

Abstract

Two isolated, hingeless rotors with identical fiber-reinforced composite root flexures were tested in hover and forward flight at realistic tip speeds. The rotors differed in blade planform and structure. The first blade set was of rectangular planform. The second set had blades of stiffer construction with swept-tips. The purpose of these tests was to measure the isolated rotor aeroelastic stability of bending/torsion coupled rotor blades over a range of flight conditions. The two soft inplane rotor systems were designed with low first torsion frequency to emphasize the effects of torsion. Regressing lag mode damping is shown in hover with precone and collective pitch variations and in forward flight with airspeed, shaft angle, precone and collective pitch variations. Correlation with comprehensive analysis for a number of test conditions is shown. Agreement in hover is excellent and forward flight correlation is reasonably good.

Introduction

The development of accurate analytical methods for aeroelastic stability prediction requires careful comparison of calculations with experimental measurements. These methods, particularly at an early stage in their development, benefit from test data obtained with simplified rotor models whose properties are accurately characterized. The U.S. Army Aeroflightdynamics Directorate, AFDD, has conducted a number of experimental investigations of this type to study aeroelastic phenomena of cantilever rotor blades. One important simplification that has enabled researchers to concentrate on the structural dynamics and aerodynamics of the rotor system has been to isolate the rotor from hub motion. Early work with isolated rotors simplified the experiment to Froude-scaled tip speeds in hover. A logical progression of structural models has been tested under these conditions. Initial work with rigid blades, tailored flap and lead-lag flexures and high torsion stiffness was reported in references 1-3. This work was further expanded in references 4-6 to investigate the effects of several design parameters on hingeless rotor stability. In addition, reference 4 emphasized the influence of torsion on the aeroelastic stability problem by designing a model with a low first torsion frequency. Design parameters for bearingless hubs were tested in references 7 and 8. These experiments added the complexity of the bearingless hub while retaining simple airfoil and planform design for the blade. References 6 and 8, while not primarily isolated rotor tests, are included here because a portion of each test was for an isolated rotor.

Aeroelastic stability investigations of isolated rotors at the AFDD were first extended to forward flight in an experimental test by McNulty.[9] This hingeless rotor had discrete flap and lead-lag flexures, a rigid blade, and high

Presented at the American Helicopter Society 55th Annual Forum, Montreal, Quebec, Canada, May 25-27, 1999.

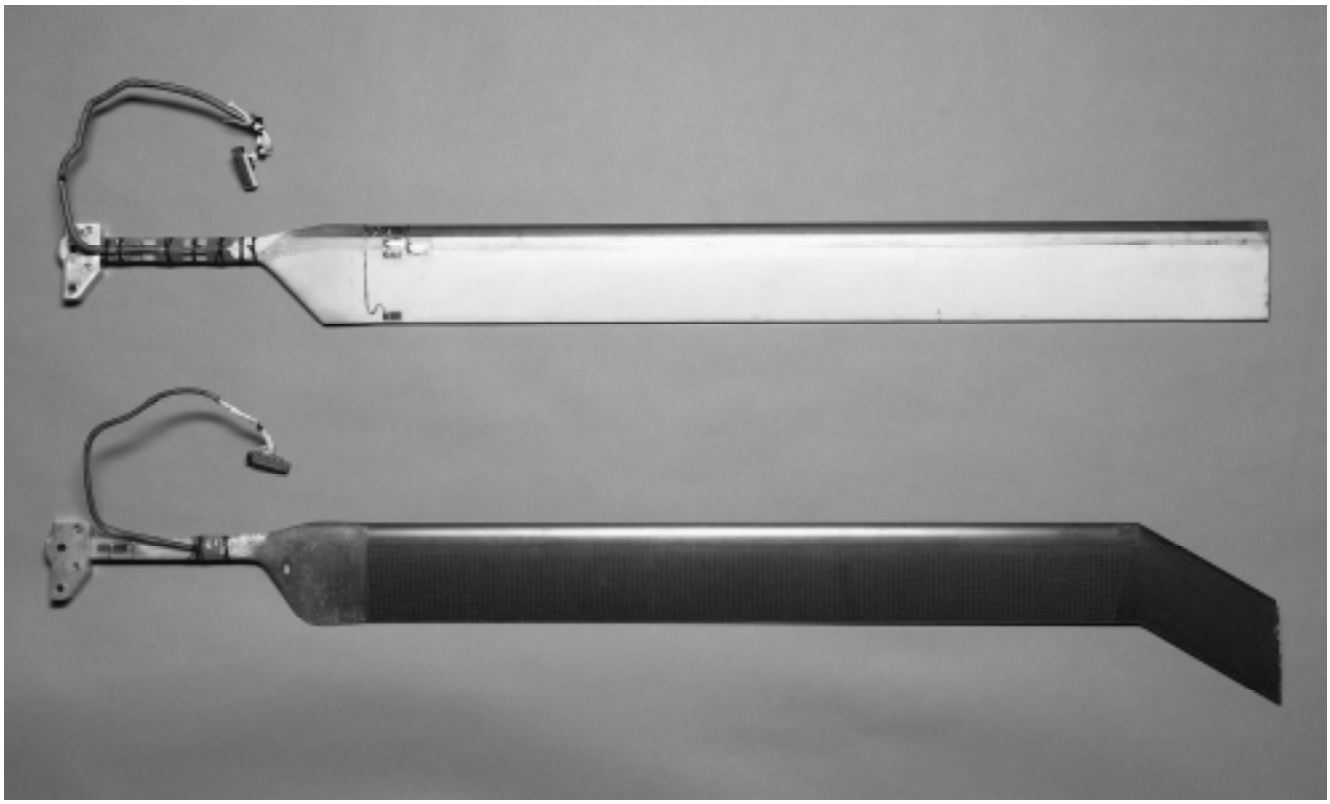

Fig. 1 Straight and swept-tip instrumented rotor blades.

torsional stiffness.

In 1995 the first of two Mach-scaled rotor tests designed to provide data for analytical code validation in forward flight was completed. A 7.5 foot diameter, hingeless rotor with straight blades was tested at the AFDD. The test data and comparison with analytical models were reported in references 10 and 11. The second test with a 7.5 foot diameter, hingeless rotor with swept-tip blades has now been completed. The swept-tip geometry introduces additional bending/torsion coupling and provides data which amplify the importance of the airloading at the tip of the blade. The model rotor experiments were designed to test the capability of current and future analytic predictive tools. For this reason the structural and aerodynamic designs were chosen to minimize the unknowns and/or approximations required by the analyst. Particular attention was paid to the pitch bearing design to avoid contamination of the aeroelastic stability with structural and kinematic nonlinearites.

This paper presents a short description of the rotors, briefly discusses the structural testing of the blades, and describes the hover and forward flight testing. Data from the tests are presented and compared with calculations from a comprehensive rotor code, CAMRAD II[12].

Model Description

Both hingeless rotors are 7.5 feet in diameter, with a 3.4 inch chord, zero pre-twist and NACA 0012 airfoil section. Solidity of both rotors is 0.096. Two hub precone angles were tested, 0° and 2°. The nominal rotor speed of 1700 RPM results in a Reynolds number of 1.2×10^6 and a Mach number of 0.60 at the blade tip in hover.

Blades from the two rotors are shown in figure 1. The most significant difference between the blades is the planform. The swept-tip blade has 30° of aft sweep over the outer 10% of the blade. In the swept region the airfoil section is

translated or sheared back as a NACA 0012 airfoil section perpendicular to the un-swept leading edge. Therefore, the chord length relative to the local leading edge in the swept region is 3.4 inches times the cosine of 30°, or 2.94 inches.

Another difference apparent in figure 1 is the color of the blade skin. The straight blade is predominately light in color due to the E-glass skin, however, it has a strip of black along the airfoil leading edge. This contrasts the black color of the entire airfoil section of the swept-tip blade. This points to significant structural differences between the two blades. The straight blade has a strip of uni-directional carbon along the airfoil leading edge to help locate the tensile axis near the center of gravity and hence reduce steady chordwise moments. The swept-tip blade has a ply of woven carbon fabric oriented at +45°/-45° to the local leading edge over the entire blade airfoil. This was added to increase the torsional stiffness of the blade. The increase in torsional stiffness was desirable to offset the increased polar moment of inertia resulting from the geometry of the tip sweep. In this way, the first torsion frequency of the swept-tip blade was similar to the frequency of the straight blade.

Similarities between the two blades include the root flexure and the general design concept. Both blades are built around a spar which wraps around the root lug and extends straight out to the tip of the straight blade and until the spar meets the leading edge inner skin surface of the swept-tip blade. The spar has a woven E-glass tube around the outer surface in the root flexure region. This tube forms a +45°/-45° outer ply to increase the torsional stiffness of the flexure. The design of the straight blade sections of both blades is also very similar in concept. Rigid foam is bonded to the spar to form the airfoil shape. Segmented leading edge weights are bonded to the leading edge foam to help bring the center of gravity forward. The airfoil skin consists of three plys of woven fabric over the entire airfoil and a strip of uni-directional carbon over the leading edge. This carbon strip is covered by a thin ply of E-glass fabric to improve the surface finish. Although conceptually similar, the specific material used for the skin is different in the two blade structures. The straight blade has three plys of 0.005 inch E-glass. The swept-tip blade has an upper and lower ply of 0.002 inch E-glass, and a ply of 0.005 carbon in the center. In both cases the upper and lower plys are oriented at 0°/90° to the leading edge and the center ply is oriented at +45°/-45°. The transition from the root flexure to the blade section of both blades has additional E-glass plys to locally stiffen the structure.

The structure of the swept section of the swept-tip blade has some similarity to the constant blade sections, however, these are limited to the skin and core materials. The number and orientation of the skin plys for the swept section are the same as the constant blade sections. The outer and inner E-glass plys are replaced with 0.005 carbon, having the same 0°/90° orientation. The middle ply is 0.005 inch carbon, as it was in the constant section of the swept-tip blade. The swept region has no uni-directional carbon strip, a single 0.109 lb. leading edge weight replacing the segmented leading edge weights and there is no spar outboard of 93% span.

Structural property measurements for the straight blades were described in ref. 10. Similar measurements were made for the swept-tip blades. It was not possible with the swept-tip blades to measure the mass properties of the straight section on every blade. Therefore, one test blade was cut up to measure the mass properties and tensile axis of the straight section. It also was not possible to measure bending and torsion stiffness in the short swept section, so a special two-foot long section was made for this purpose. Due to cost constraints this section was made to match the cross-section normal to a straight radial line with the skin fabric wrapping around the leading edge. Therefore, it is not the exact structure of the swept section. The properties used in the analysis shown in this paper for the swept section were measured from this specimen and transformed to the 30° swept axis. The transition from straight to swept blade was another difficulty not present with the straight blade. It was assumed that the stiffness changes in the transition were negligible, but that the mass properties should be accurately captured. To accomplish this, all the weight and moment of inertia changes from the straight and swept section properties were incorporated into a single lumped mass. This lumped mass is dominated by the large leading edge weight located just inboard of the initiation of sweep. This leading edge weight was designed to offset the weight of the swept section and place the entire blade center of gravity at the straight blade section quarter chord.

Fig. 2 Swept-tip rotor on RTR test stand in the Army/NASA 7- by 10-Foot Wind Tunnel.

The swept-tip rotor system may be seen as installed in the Army/NASA 7- by 10-Foot Wind Tunnel #1 in figure 2. The blades are attached to a hingeless rotor hub which was designed for these rotor tests. The feathering bearings are stacked ball bearings which were chosen for the minimal additional damping that they introduced to the system. Rotor control is achieved through a conventional swashplate which applies pitch on the blade root cuff inboard of any flap or lag flexure motion, resulting in negligible root end kinematic coupling. Fundamental blade flap and lag motion is accommodated with the composite root flexure that was described above.

The natural frequencies of the straight and swept-tip rotor systems are shown in figures 3 and 4, respectively. The symbols show rotating and non-rotating measurements, and the curves represent calculations using the CAMRAD II eigenvalue analysis simulating *in-vacuo* conditions at 0° collective pitch angle. Non-rotating frequencies were measured with the root fitting rigidly clamped to a massive, rigid structure. Rotating frequencies were only measured for the first lag mode and the data shown is for a range of collective pitch angles. The fundamental flap, lag and torsion frequencies calculated with CAMRAD II at the operating speed of 1700 RPM were 1.13, 0.71 and 2.56 cycles/revolution for the straight blade and 1.12, 0.66 and 2.86 cycles/revolution for the swept-tip blade. The torsion frequency of the swept-tip blade is highly coupled with the second flap mode at the operating speed, so there are two modes with significant torsion motion. The second coupled flap/torsion mode frequency is calculated to be 3.27 cycles/revolution. The second flap mode of the

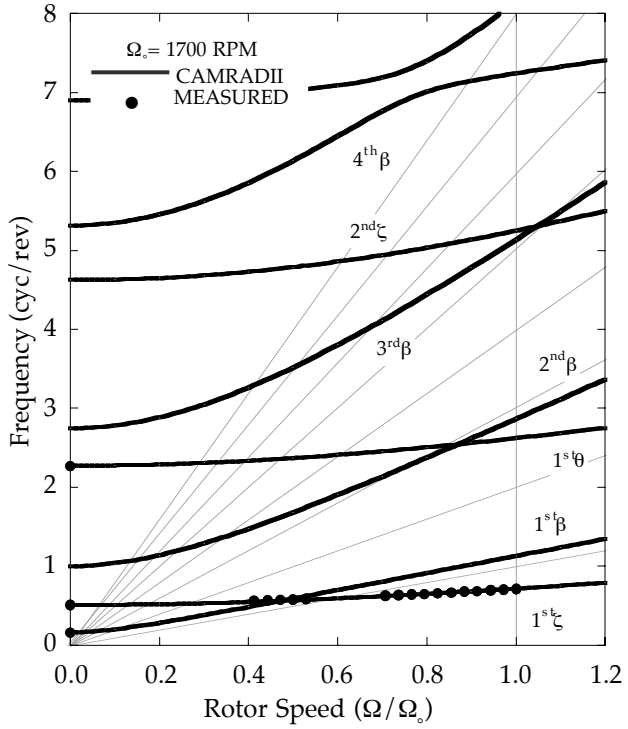

Fig. 3 Straight blade rotating frequencies diagram.

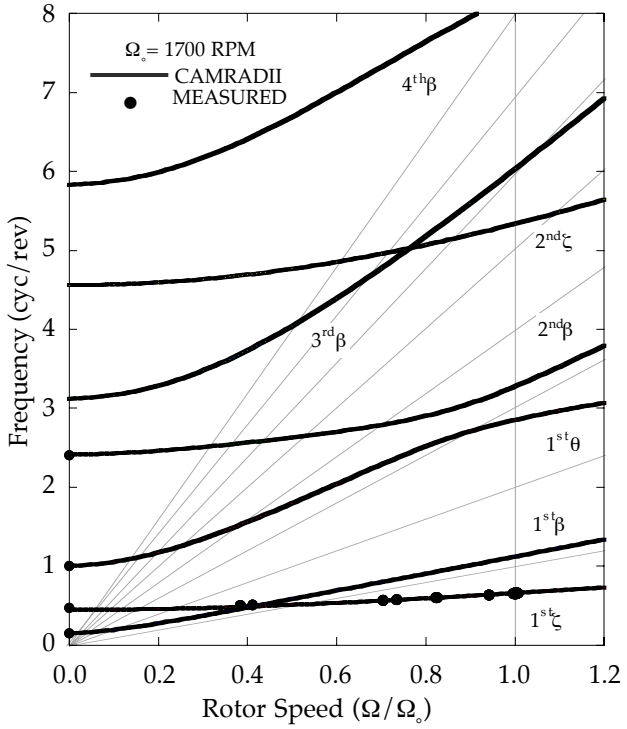

Fig. 4 Swept-tip blade rotating frequencies diagram.

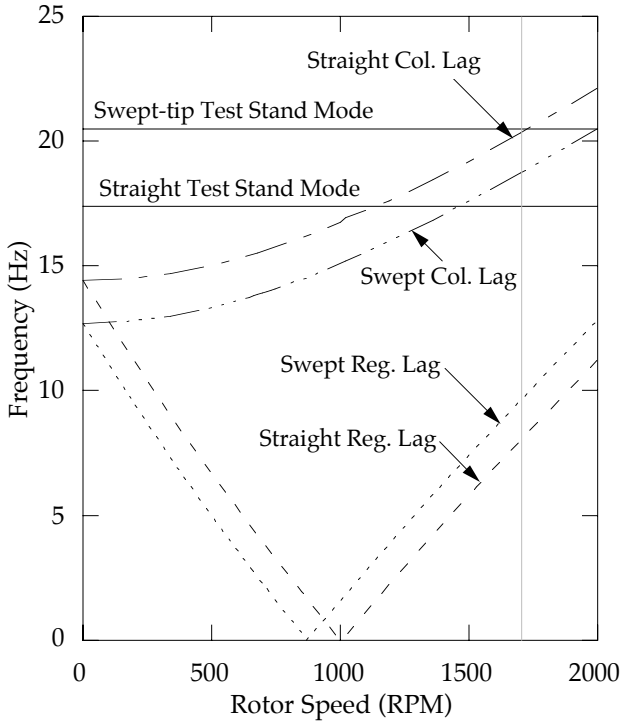

Fig. 5 Fixed system stand and rotor frequencies.

swept-tip blade is significantly higher than the straight blade. In fact, the second flap mode of the swept-tip blade is above 3 cycles/revolution at the operating rotor speed.

Measured test stand frequencies are shown in figure 5 with the calculated fixed system rotor frequencies which are nearest to the stand frequencies for the 2 rotors. Only the lowest stand frequency is shown for simplicity. The regressing lag mode frequency separation from the lowest stand frequency was 9.2 Hz for the straight blade rotor and 10.7 Hz for the swept-tip rotor at the operating rotor speed of 1700 RPM. The increase in separation for the swept-tip rotor was achieved by locking the stand in the lateral direction below the tunnel floor. This introduced significant operational difficulties because it prevented the ability to tilt the shaft without removing the tunnel floor plates and unlocking the stand first. The rotor/stand frequency separation was less than that suggested in reference 5 for a two-bladed rotor, but it was felt that these frequencies could not be raised further without major redesign of the stand. The agreement between rotating frequency measurements and CAMRAD II calculations, shown in figures 3 and 4, indicate that the stand influence is slight for these four-bladed rotors.

Dynamic stability testing requires some means of exciting the mode or modes of interest. This was achieved during these tests by using capability in the test stand. The test stand, originally built by Sikorsky Aircraft for NASA, and designated the Rotor Test Rig (RTR), had been designed to include higher harmonic swashplate control. To accomplish this, low authority, high-speed hydraulic actuators were placed in series with each of the three high authority rotor trim control electric actuators. For these tests, only one of the three hydraulic actuators was used to provide cyclic excitation at the regressing lag mode frequency through the fixed system swashplate.

Instrumentation

The model instrumentation consisted mainly of blade strain gauges. Common to both rotor tests were flap, lag, and torsion strain gauge bridges on all blades at 12% radius. Blade pitch angle was measured at the root fitting on blades #1 using a rotational potentiometer. Fixed system lateral and longitudinal acceleration just below the rotor hub were measured for safety and for rotor mass balancing. Shaft attitude was also measured. Local pressure and temperature were recorded during the hover test. During the wind tunnel test, static and dynamic pressure as well as temperature were recorded with the other data. Rotor speed and azimuthal phase relations were obtained using a once per revolution optical encoder. The encoder was positioned to produce a spike when blade #1 was over the tail of the model, and the blade sequence going clockwise looking from above was: #1, #2, #3, #4.

The RTR test stand has a fixed-system rotor balance. Unfortunately, with the balance flexibility included the lowest stand natural frequencies were very close to the rotor regressing lag frequency. Therefore, to improve the isolation of the rotor from the stand dynamics, it was necessary to lock out the balance. Structure was added to the test stand to bridge the balance, raising the stand frequencies above the regressing lag frequency.

Data Acquisition and Analysis

Simultaneous data were acquired for each rotor sensor over a period of 2 seconds at a sample rate of 1024 samples/second for the straight blade

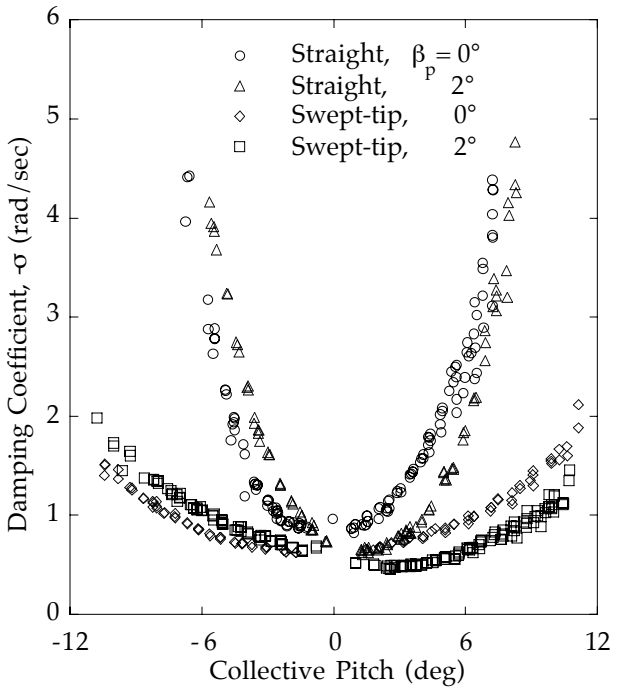

Fig. 6 Hover test regressing lag mode damping versus collective pitch angle.

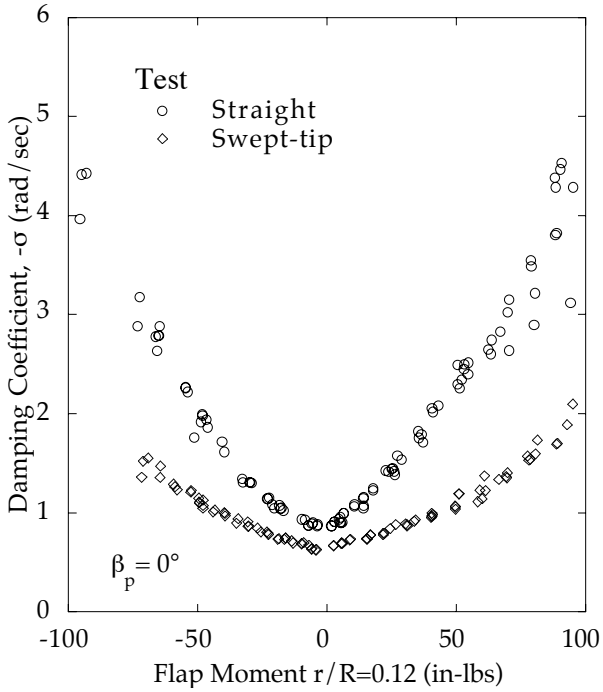

Fig. 7 Hover test regressing lag mode damping versus steady root flap moment with 0° precone hub.

rotor and 2048 samples/second for the swept-tip rotor. The voltage measurements were digitized and the strain gauge measurements were converted to bending moments based upon previous physical calibrations. The four individual blade root bending moments were transformed into the fixed system using the method of multiblade coordinates.[13] Individual rotating blade and non-rotating multiblade coordinate time history data were later analyzed for modal damping and frequency using the moving-block analysis technique.[14,15]

Hover Test Description

Hover testing of both rotors was performed in the AFDD Anechoic Hover Test Chamber. This test chamber has a rectangular planform 26 feet by 32 feet and is 28 feet in height. Inflow for the rotor is drawn into the chamber through ten 2 foot by 6 foot ducts located along the ceiling. Recirculation can be reduced by passing the rotor wake through an annular diffuser located on a moveable platform, and exhausting the flow out of the chamber along the floor on opposite sides of the room.

When acquiring data in hover the shaft angle was set to zero degrees. The rotor was set to the desired rotor speed and collective pitch angle. Low amplitude cyclic pitch excitation was applied and the frequency was adjusted until the lead/lag response of blade #1 reached a maximum. The amplitude of excitation was then adjusted to give lead/lag response just below the structural limit. The excitation was stopped and 2 seconds of data were acquired.

Hover Test Data

The regressing lag mode damping measurements for both blade sets and both hub configurations versus collective pitch in hover may be seen in figure 6. In both cases the 2° precone hub moves the data down and to the right as previous hover data and analyses have shown. The large reduction in damping with the swept-tip blades is the most obvious feature in the figure. It was first thought that the large difference in damping measured between the two rotors was due to a reduction in thrust on the swept-tip rotor compared to the straight blade rotor. Lift on the swept region of the blade creates a nose down moment along the length of the blade. This moment reduces the effective collective pitch by twisting the blade and the very soft torsion root flexure. Since thrust was

Table 1. Straight blade rotor with 0° precone hub advance ratio range for shaft angles and collective pitch angles.

	1700 RPM	
$\beta_p = 0°$	$\alpha_s = -3°$	$\alpha_s = 0°$
$\theta_o = 1.1°$	-	.01 - .36
$\theta_o = 3.4°$	.01 - .31	.00 - .19

Table 2. Straight blade rotor with 2° precone hub advance ratio range for shaft angles and collective pitch angles.

	1700 RPM		
$\beta_p = 2°$	$\alpha_s = -6°$	$\alpha_s = -3°$	$\alpha_s = 0°$
$\theta_o = 2.9°$	.00 - .31	.01 - .31	.00 - .31
$\theta_o = 3.2°$	-	.02 - .36	-
$\theta_o = 3.8°$	.00 - .31	.01 - .31	-
$\theta_o = 4.2°$	-	.02 -.41	-
$\theta_o = 4.8°$	.00 - .33	.00 -.30	-
$\theta_o = 5.2°$	-	.03 -.36	-
$\theta_o = 5.9°$	.04 - .36	-	-

not measured the steady flap moment at 12% span was used to assess this theory. Figure 7 shows the damping versus steady flap for both rotors with the 0° precone hub. The damping measurements move slightly closer to one another when shown versus flap moment, however, it is apparent that there is another mechanism responsible for the difference in damping for these two rotors.

Forward Flight Test Description

Forward flight testing took place in the AFDD 7- by 10-Foot Wind Tunnel #2 for the straight blade rotor and the Army/NASA 7- by 10-Foot Wind Tunnel #1 for the swept-tip rotor. The Wind Tunnel #2 was taken out of commission shortly after the straight blade test was completed and was, therefore, not available for the swept-tip test. Differences between the two tunnels are few in that they were built to the same specification at the same time. Modifications have been made to the tunnels over the years, the most significant of which was the addition of flow control screens in the Wind Tunnel #1.

When acquiring data in forward flight the shaft angle was set, the rotor speed brought up to 1700 RPM, collective pitch was set and the tunnel airspeed was slowly increased to the desired value

Table 3. Swept-tip rotor with 0° precone hub advance ratio range for shaft angles and collective pitch angles.

	1700 RPM			1500 RPM
$\beta_p = 0°$	$\alpha_s = -6°$	$\alpha_s = -3°$	$\alpha_s = 0°$	$\alpha_s = 0°$
$\theta_o = 2°$	-	-	.30	-
$\theta_o = 3°$	.00 - .46	.04 - .46	.00 - .46	-
$\theta_o = 4°$	.05 - .46	.01 - .46	.00 - .46	.10 - .51
$\theta_o = 5°$	.01 - .45	.01 - .41	.01 - .46	-
$\theta_o = 6°$	.10 - .46	.10 - .46	.10 - .46	-
$\theta_o = 7°$	-	-	.15 - .41	-
$\theta_o = 8°$	-	-	.30	-

Table 4. Swept-tip rotor with 2° precone hub advance ratio range for shaft angles and collective pitch angles.

	1700 RPM		
$\beta_p = 2°$	$\alpha_s = -6°$	$\alpha_s = -3°$	$\alpha_s = 0°$
$\theta_o = 2°$	-	-	.30
$\theta_o = 3°$	.02 - .46	.00 - .47	.01 - .46
$\theta_o = 4°$	.10 - .46	.02 - .46	.10 - .46
$\theta_o = 5°$	.10 - .46	.15 - .46	.10 - .46
$\theta_o = 6°$	.10 - .46	.10 - .46	.10 - .46
$\theta_o = 7°$	-	-	.30
$\theta_o = 8°$	-	-	.30

while the rotor cyclic pitch was adjusted to maintain low oscillatory flapping loads. Having established the desired air speed, the collective was re-adjusted to get as close as possible to the desired value and the cyclic pitch adjusted to minimize the 1P flapping moment at 12% radius on blade #1. Low amplitude cyclic excitation was applied and the frequency was adjusted until the lead/lag response reached a maximum. The amplitude of excitation was then adjusted to give lead/lag response just below the structural limit. The excitation was shut off and 2 seconds of data were acquired. The forward flight test envelope for which data were collected is shown in Tables 1-4. There is a separate table for each combination of blade type (straight or swept-tip) and hub precone angle (β_p=0° or β_p=2°). In the tables the range of advance ratio for different shaft angles, α_s (positive aft), and collective pitch angles, θ_0, are shown.

In references 10 and 11 lag mode damping measurements for the straight blade test have been shown for the regressing lag frequency of a

multiblade cyclic mode. During the course of the swept-tip wind tunnel test the damping of blade #1 changed significantly. The reason for this change has not been determined. The other three blades did not experience a similar change. In figure 8, damping measurements from blade #1 and blade #3 are shown versus advance ratio with the 2° precone hub. The rotor was set at 0° shaft angle and approximately 3° collective pitch angle. The measurements were acquired on three different days. The data with open symbols were acquired early in the test up to an advance ratio of 0.35. The operating envelope was later expanded and additional data were acquired from μ=0.35 to μ=0.46, shown as gray symbols. A step may be seen between these two data sets for both blades, however, the step seen in the blade #1 data is much greater than blade #3. The solid symbol data was acquired on the second to last day of testing. Differences seen in the blade #1 data appear to be much more significant than the differences seen in the blade #3 data. Rather than smear the damping changes of blade #1 into the entire database by showing the multiblade cyclic mode, rotating measurements from blade #3 are shown for the rotor with swept-tip blades. Measurements on blades #2 through #4 were all very similar, but blade #3 was chosen because it had the lowest structural damping.

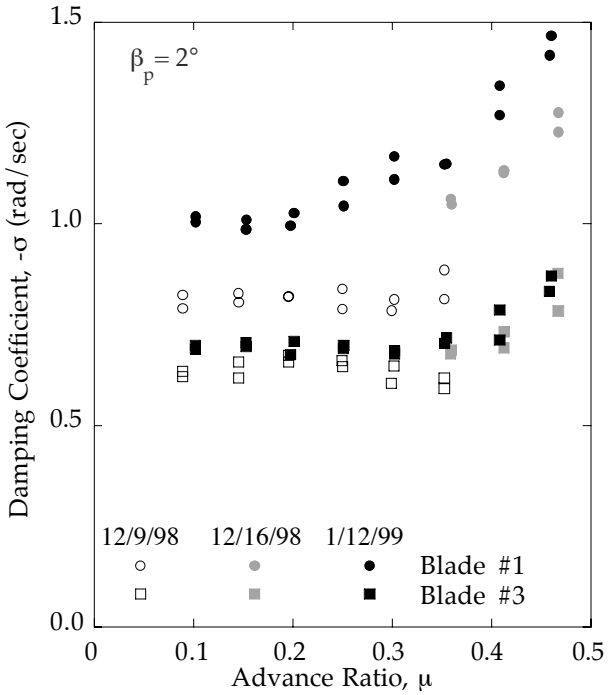

Fig. 8 Swept-tip blade forward flight test individual blade lag mode damping versus advance ratio for 3 different days during the test; 0° shaft angle, 3° collective pitch angle.

Forward Flight Test Data

Operating conditions for the swept-tip rotor were chosen to match conditions that had previously been acquired with the straight blade rotor. These conditions were specified in terms of collective pitch angle, shaft angle and advance ratio. The thrust of the two rotors was not measured and, therefore, not used to specify the operating conditions. Once data had been acquired with the swept-tip blades for all of the conditions that had been previously acquired with the straight blades the test conditions were expanded to additional advance ratios and collective pitch angles. For the results shown here, a least squares polynomial curves fit has been shown with the data to better illustrate trends.

Damping measurements for three shaft angles with 3° collective pitch on the straight blades with the 2° precone hub showed a significant change in damping with advance ratio. In fact, a neutral stability speed was encountered with 6° of forward (or negative) shaft tilt. Measurements for both rotors at three shaft angles, α_s = 0°, –3°, and –6°, are shown in figures 9 and 10. Below μ = 0.30, the damping levels measured on the swept-tip blades were significantly lower than on the straight blades. No significant reduction in damping with advance ratio is seen for any of the shaft angles on the swept-tip blades. The swept-tip data extends significantly past the straight blade data in advance ratio and the damping level for all three shaft angles shows an increase in damping beyond μ=0.35.

An effort was made to acquire a family of advance ratio sweeps for different collective pitch angles at all three shaft angles. It was only possible to acquire a family of advance ratio sweeps for different collective pitch angles by testing with forward shaft tilts greater than 0° on the straight blade rotor. The swept-tip rotor did not suffer the same limitation. At –6° shaft angle with the straight blade rotor data were acquired for four collective pitch angles where all sweeps reached an advance ratio of 0.31. These conditions were matched with the swept-tip rotor and the measurements may be seen in figures 11 and 12. The

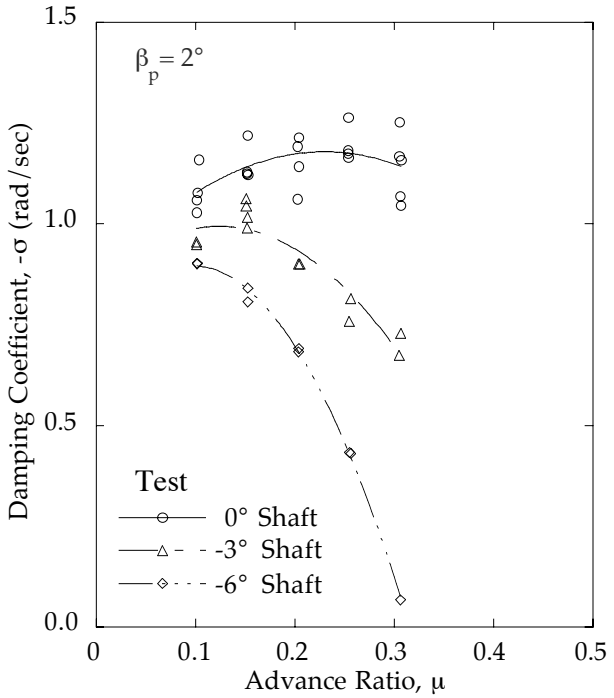

Fig. 9 Straight blade rotor forward flight test regressing lag mode damping versus advance ratio for three shaft angles at 3° collective pitch.

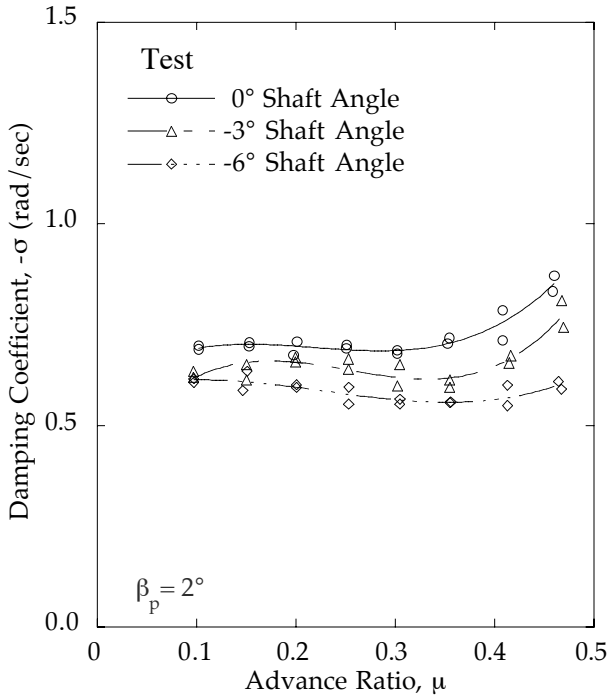

Fig. 10 Swept-tip rotor forward flight regressing lag mode damping versus advance ratio for three shaft angles at 3° collective pitch.

damping coefficient scale has been expanded from the previous figures showing shaft angle variation to show all the sweeps. The damping measurements for the straight blade rotor show greater variation with collective pitch angle and with advance ratio.

The forward shaft angle and relatively low collective pitch angles of the preceeding figures result in low thrust conditions. It was desirable to acquire data for thrust conditions more representative of helicopter flight operations where possible. The swept-tip rotor wind tunnel test was more successful toward this end. A family of damping versus advance ratio data for different collective pitch angles at 0° shaft angle were acquired up to 7° collective pitch. Figure 13 shows the data for five collective pitch angles on the 0° precone hub. These data show the strongest variation in damping with advance ratio that was measured with the swept-tip blades. A similar family, not shown here, was acquired with the 2° precone hub with four collective pitch angles up to 6°.

Collective sweeps at 0.30 advance ratio were acquired to push the swept-tip rotor to a high thrust level in forward flight. Figure 14 shows the damping measurements for the collective pitch sweeps using both 0° and 2° hub precone angles. At 8° collective pitch angle the un-perturbed loads were near the load limit leaving very little load margin for excitation. The data with both hub precone angles show smooth curves with an increasing difference between the two hub configurations.

CAMRAD II Model

The CAMRAD II structural models for both rotors have the same number of elastic elements and the elements have the same degrees of freedom. The straight blade has one element in the flexure section and five elements distributed along the remainder of the blade. The last element is 10% of span. The swept-tip blade has the identical number and distribution of elastic elements. Modal structural damping was adjusted to agree with the hover measurements near 0° collective pitch angle individually for both rotors. The values of modal damping were 0.38% Cr for the straight blade and 0.32% Cr for the swept-tip blade.

The aerodynamic model in CAMRAD II is described in detail in reference 12. Both straight

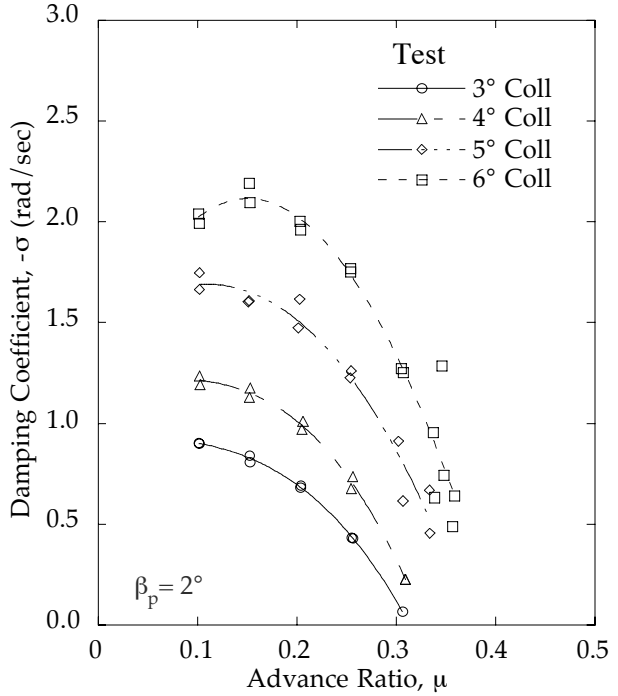

Fig. 11 Straight blade rotor forward flight test regressing lag mode damping versus advance ratio for four collective pitch angles with -6° shaft angle.

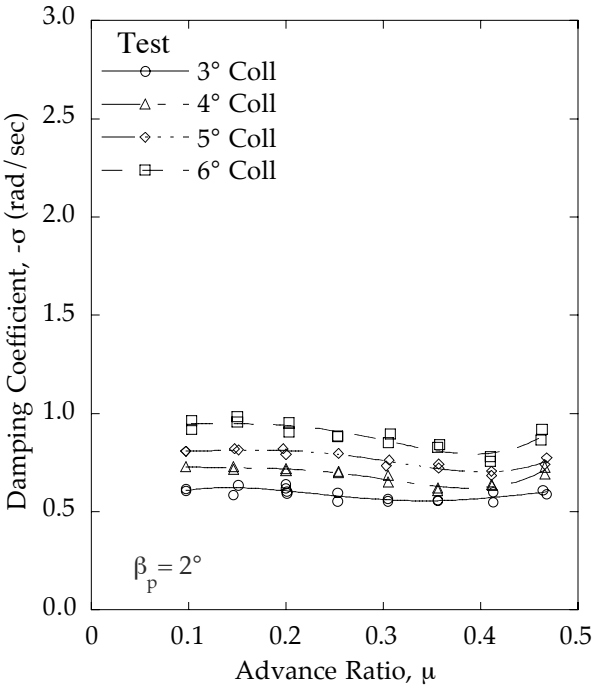

Fig. 12 Swept-tip rotor forward flight test regressing lag mode damping versus advance ratio for four collective pitch angles with -6° shaft angle.

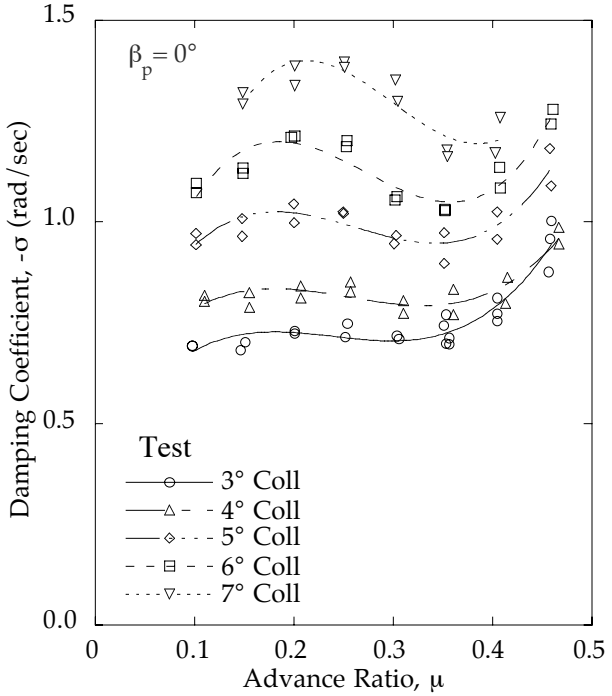

Fig. 13 Swept-tip rotor forward flight test regressing lag mode damping versus advance ratio for five collective pitch angles with 0° shaft angle.

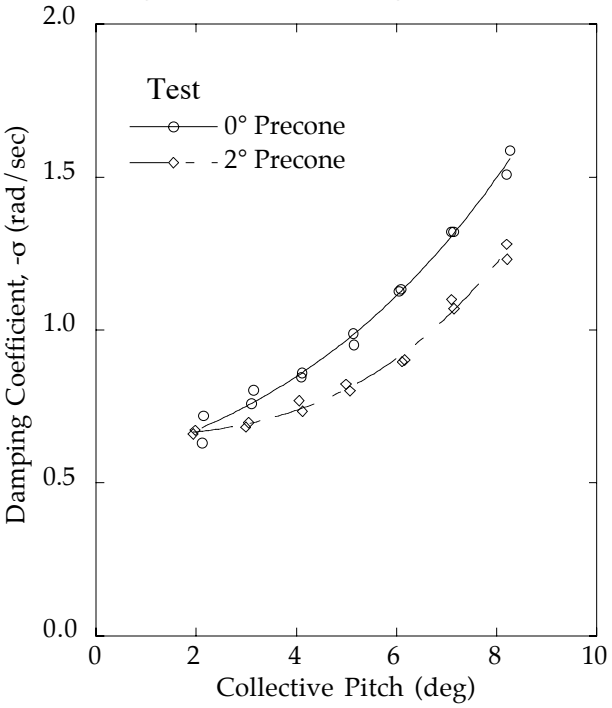

Fig. 14 Swept-tip rotor forward flight test regressing lag mode damping versus collective pitch angle for two hub precone angles at 0.30 advance ratio.

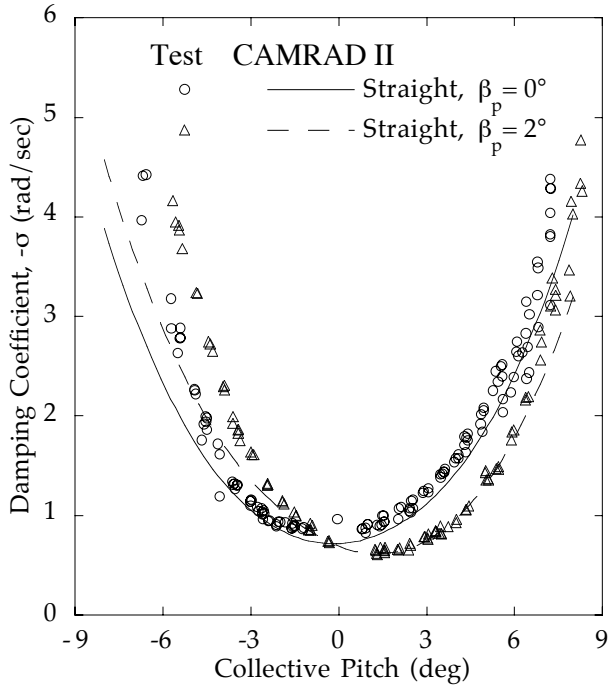

Fig. 15 Comparison of CAMRAD II calculated and measured hover regressing lag mode damping versus collective pitch angle for straight blade with two precone angles.

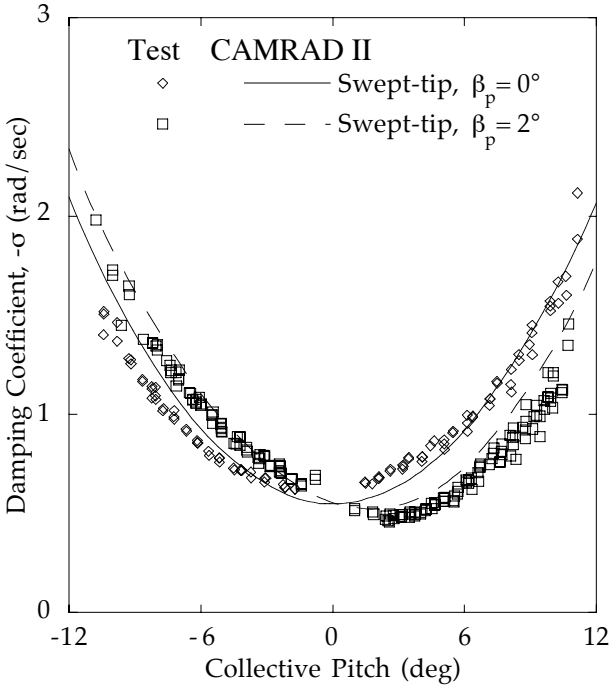

Fig. 16 Comparison of CAMRAD II calculated and measured hover regressing lag mode damping versus collective pitch angle for swept-tip blade with two precone angles.

and swept-tip blades are divided into 15 aerodynamic segments and an NACA 0012 C81 airfoil table provided lift, drag and moment with angle of attack and Mach number. The baseline calculation for hover used uniform inflow with a hover inflow correction factor equal to 1.1, tip loss equal to 0.98 for trim and the three-state momentum theory dynamic inflow model for the flutter analysis. Forward flight calculations were made with the free wake inflow model for trim and the three-state Pitt and Peters dynamic inflow model for the flutter analysis.

Comparison of Theory and Test Data

Calculated results for hover using CAMRAD II are shown with test data in figures 15 and 16 for the straight and swept-tip rotors, respectively. The correlation is better for the positive collective pitch angles than for the negative angles. The data show slightly higher damping for negative collective pitch angles than for positive collective pitch angles and this is not present in the calculations.

Three inflow models are shown in figure 17 for the swept-tip rotor with the 2° precone hub.

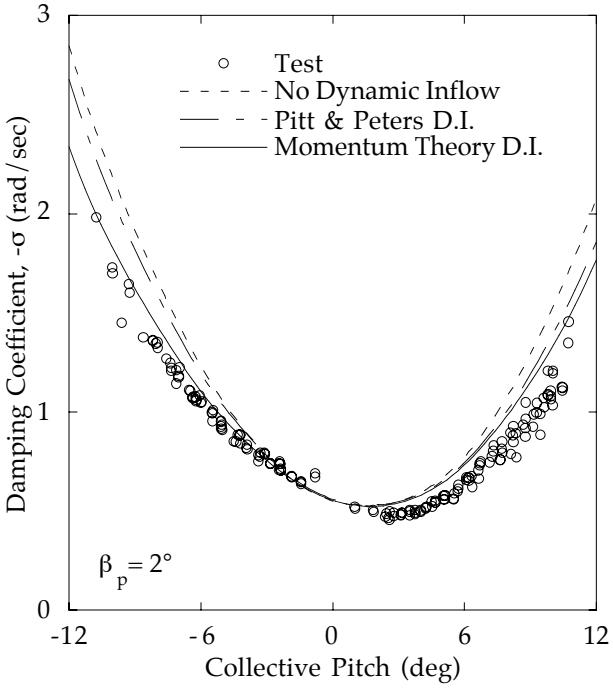

Fig. 17 Comparison of CAMRAD II calculations with three inflow models and measured hover regressing lag mode damping versus collective pitch angle; swept-tip blade with 2° precone hub.

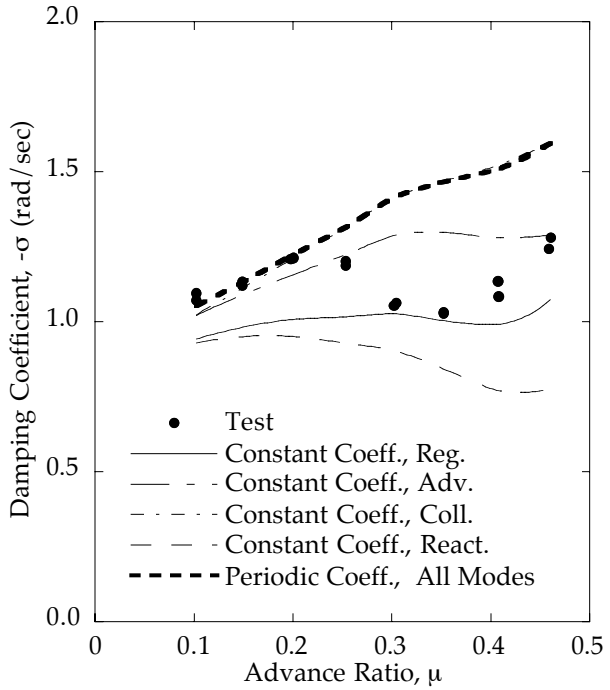

Fig. 18 Comparison with swept-tip rotor of measured forward flight regressing lag mode damping, and 2 CAMRAD II solution methods; 0° shaft angle, 6° collective pitch angle, 0° precone hub.

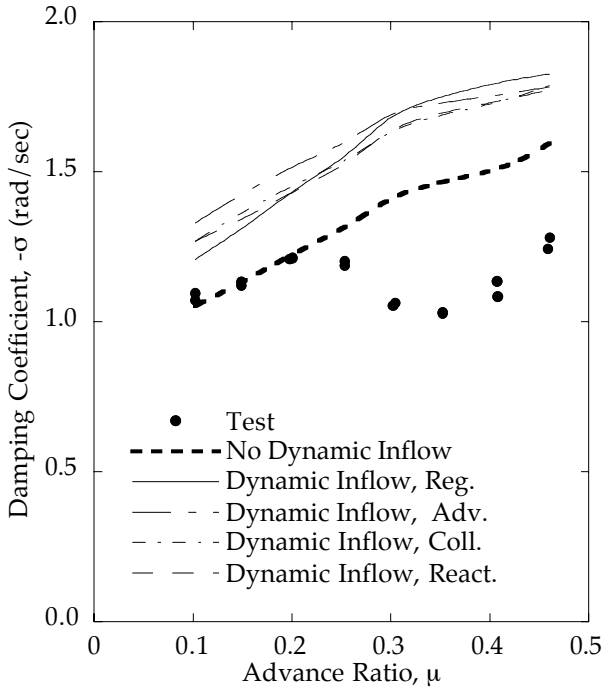

Fig. 19 Comparison with swept-tip rotor of measured forward flight regressing lag mode damping, CAMRAD II periodic solution without dynamic inflow and CAMRAD II periodic solution with dynamic inflow; 0° shaft angle, 6° collective pitch angle, 0° precone hub.

The models include, no dynamic inflow, Pitt and Peters dynamic inflow and a momentum theory dynamic inflow model. Both dynamic inflow models contain three states. The differences due to these inflow models are small. The momentum theory dynamic inflow model shows the best correlation with the data, however, there are other modeling parameters such as the inflow factor and tip loss parameter which could change this conclusion.

Calculations shown for hover are, of course, for a constant coefficient set of equations. In forward flight the equations are periodic. At low speed the periodicity is weak and solving averaged constant coefficient equations may be sufficient. As forward speed increases, this approximation may be unsuitable. Figure 18 shows a comparison of test measurements, a constant coefficient approximate solution and the periodic Floquet solution for a forward flight speed sweep. The test configuration with the swept-tip rotor on the 0° precone hub is 0° shaft tilt, 6° collective pitch and advance ratio increasing from 0.10 to 0.46. Both solutions procedures are for models with no dynamic inflow or hub degrees of freedom, so one would expect to see no difference between the regressing, advancing, collective and reactionless modes. The periodic solution with no dynamic inflow shows no difference between the four multiblade modes. The constant coefficient approximation, however, gives one half the damping for the reactionless mode compared to the collective mode. The collective mode agrees well with the periodic coefficient solution over the entire speed range. The mode that was excited in the experiment, the regressing lag mode, is seen to be considerably below the periodic coefficient solution above $\mu = 0.30$. It is, therefore, not adequate to use the constant coefficient approximation for correlation with this experiment. All of the remaining calculations in this paper solve the periodic coefficient equations.

The influence of the dynamic inflow model in forward flight is shown in figure 19. The test data and periodic coefficient solution with no dynamic inflow from figure 18 are shown with the periodic coefficient solution using the three-state Pitt and Peters dynamic inflow model. The addition of dynamic inflow moves the damping of all modes up considerably. Only slight differences are seen between the individual non-rotating rotor modes,

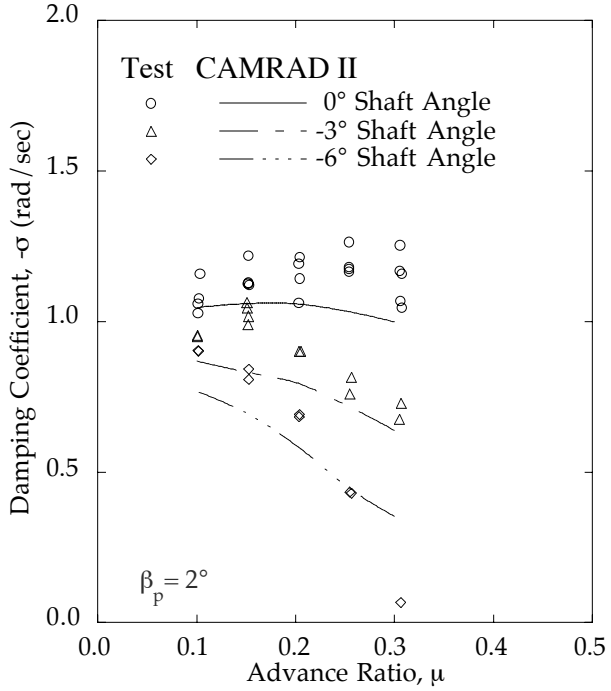

Fig. 20 Comparison with straight blade rotor of CAMRAD II calculations and measured regressing lag mode damping for three shaft angles at 3° collective pitch.

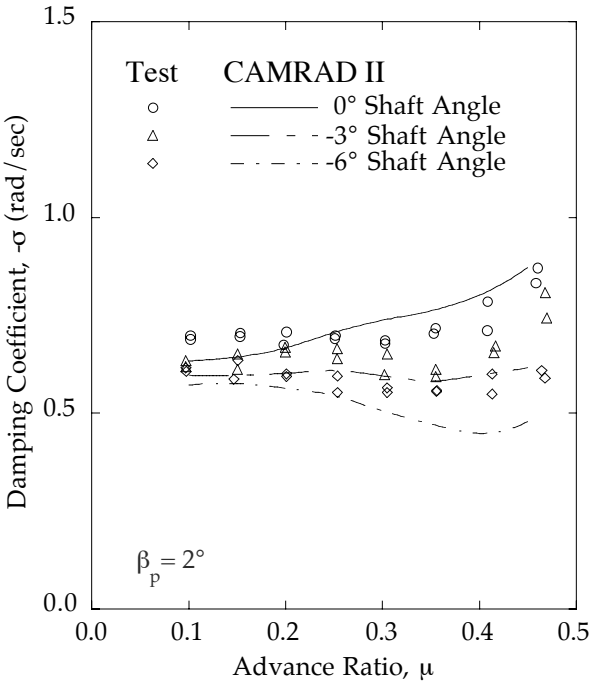

Fig. 21 Comparison with swept-tip rotor of CAMRAD II calculations and measured regressing lag mode damping for three shaft angles at 3° collective pitch.

but the major effect is an increase in the damping coefficient of all four modes.

CAMRAD II calculations have been made for all of the forward flight data shown previously in the paper. The free wake model is used for the trim solution. No attempt was made to determine the importance of the trim wake model on the solution. The rotor was trimmed to the measured cyclic control angles or to minimize the fixed system pitch and roll moment. There was no noticeable difference in the resulting damping values for the swept-tip rotor. The results shown here were trimmed to minimize the fixed system steady pitch and roll moment, as this gave better correlation with the straight blade rotor. The Pitt and Peters dynamic inflow model was used for the forward flight calculations.

Figures 20 and 21 compare calculations with lag mode damping measurements for both rotors with shaft angle variation. The calculations for the straight blade are reasonably good except for the last increment in advance ratio for –6° shaft angle. The measurement drops quickly to nearly 0 rad/sec at $\mu = 0.30$ while the calculation drops only mildly. The general spread and trend of the data is captured. The calculations for the swept-tip rotor are quite good for all 3 shaft angles, although the calculation shows greater difference in damping for the shaft variation than do the measurements.

Figures 22 and 23 compare calculations with lag mode damping measurements for both rotors with collective pitch variation at –6° shaft angle. The correlation is reasonably good for both rotors. Details which do not appear to be captured include the upward trend in damping at the highest speeds for the higher collective pitch angles with the swept-tip blade and the low damping region at moderately high speed ($\mu = 0.30$) for the straight blade rotor.

Figure 24 compares calculation with lag mode damping measurements for the swept-tip rotor with collective pitch variation at 0° shaft angle. The correlation appears to degrade with thrust. The 0° shaft angle cases with high collective pitch should be the highest thrust cases for which damping measurements were made. It appears that the damping is over predicted and that the up-down-up trend with advance ratio in the data is not captured.

Finally, figure 25 compares calculation with lag mode damping measurements for two collective

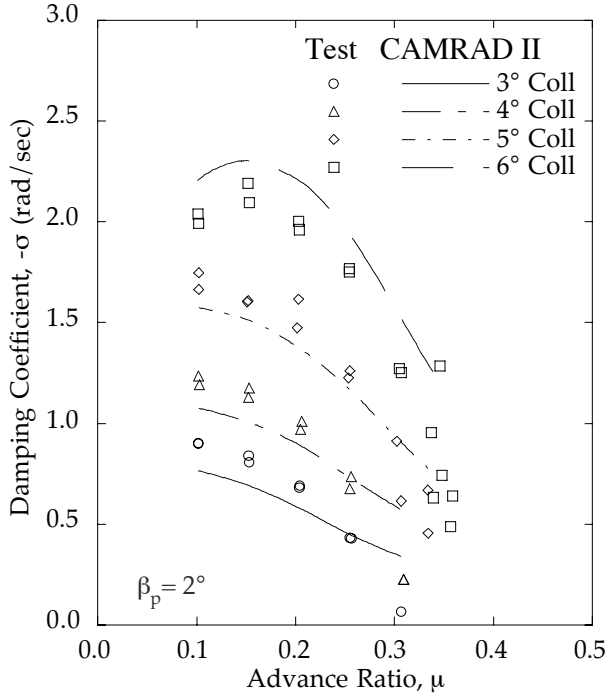

Fig. 22 Comparison with straight blade rotor of CAMRAD II calculations and measured regressing lag mode damping for four collective pitch angles at -6° shaft angle.

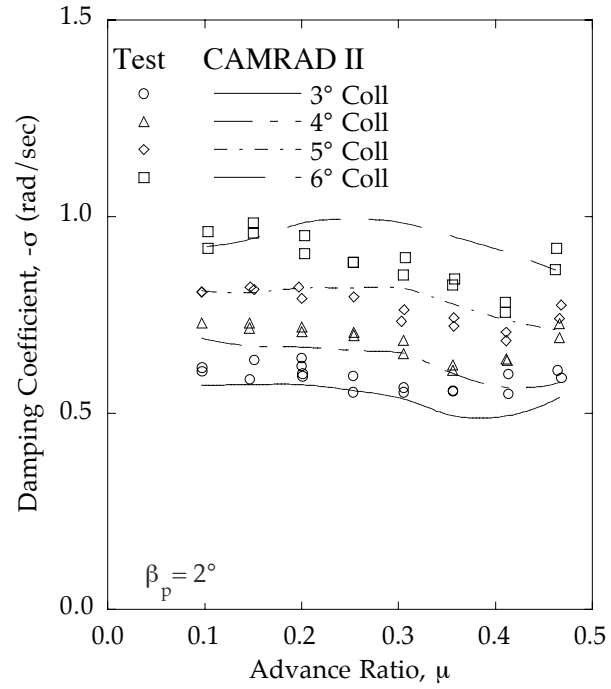

Fig. 23 Comparison with swept-tip rotor of CAMRAD II calculations and measured regressing lag mode damping for four collective pitch angles at -6° shaft angle.

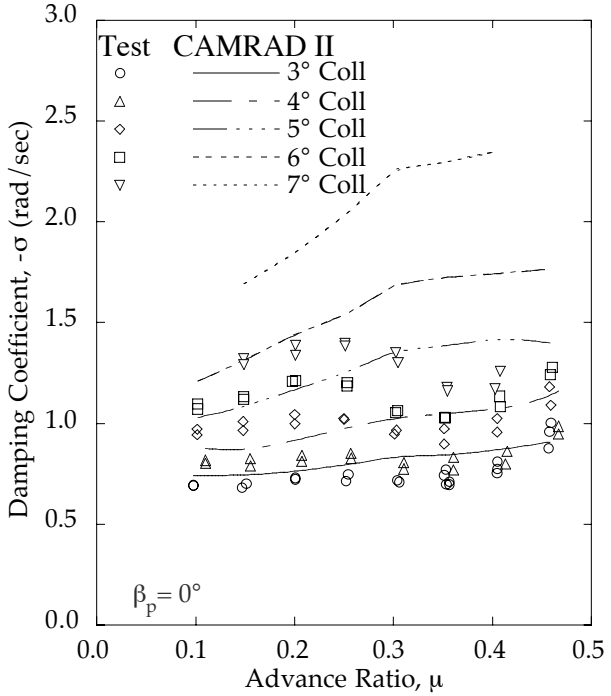

Fig. 24 Comparison with swept-tip rotor of CAMRAD II calculations and measured regressing lag mode damping for five collective pitch angles at 0° shaft angle.

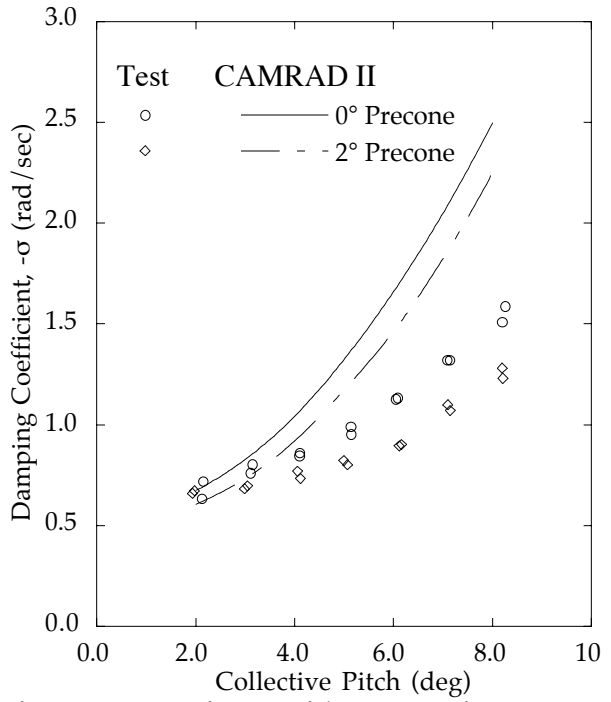

Fig. 25 Comparison with swept-tip rotor of CAMRAD II calculations and measured regressing lag mode damping over a range of collective pitch angles at 0.30 advance ratio with both precone angles.

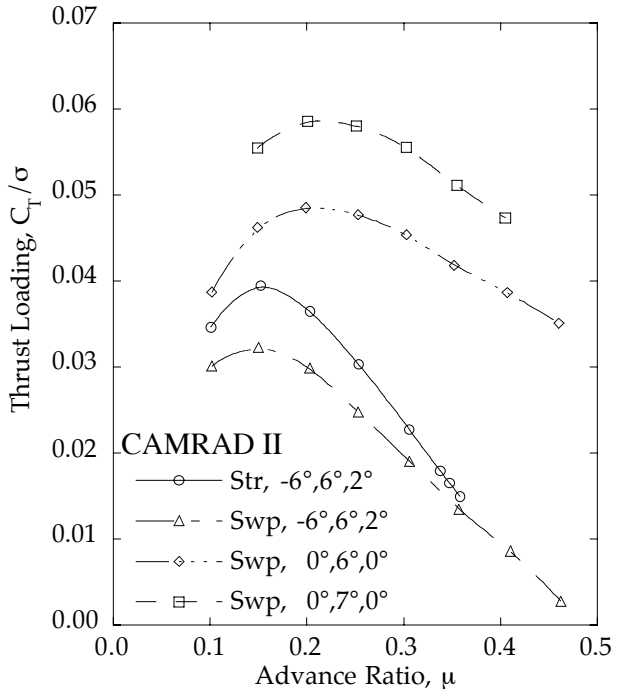

Fig. 26 CAMRAD II calculated thrust loading for four advance ratio sweeps; straight blade rotor, -6° shaft angle, 6° collective pitch angle, 2° precone; swept-tip rotor, -6° shaft angle, 6° collective pitch angle, 2° precone; swept-tip rotor, 0° shaft angle, 6° collective pitch angle, 0° precone; and swept-tip rotor, 0° shaft angle, 7° collective pitch angle, 0° precone .

pitch sweeps at 0.30 advance ratio with the swept-tip rotor. The sweeps are for the 0° and the 2° hub precone angles. The correlation seen here is consistent with the previous figure. At low collective pitch angle the correlation is excellent, but the calculations over predict the damping for both hub configurations as collective pitch is increased. The measurements show an increasing difference between the two hubs as collective pitch is increased. The calculations show this difference increasing as well.

Thrust measurements were not made during these tests; however, the thrust calculated with CAMRAD II may be used as an estimate of the operating conditions for which measurements were made. Figure 26 shows the thrust loading calculated for four advance ratio sweeps previously shown in the paper. The operating conditions are identified in the figure by listing the blade type, shaft angle, collective pitch angle, and the hub precone angle, respectively. Calculations show the

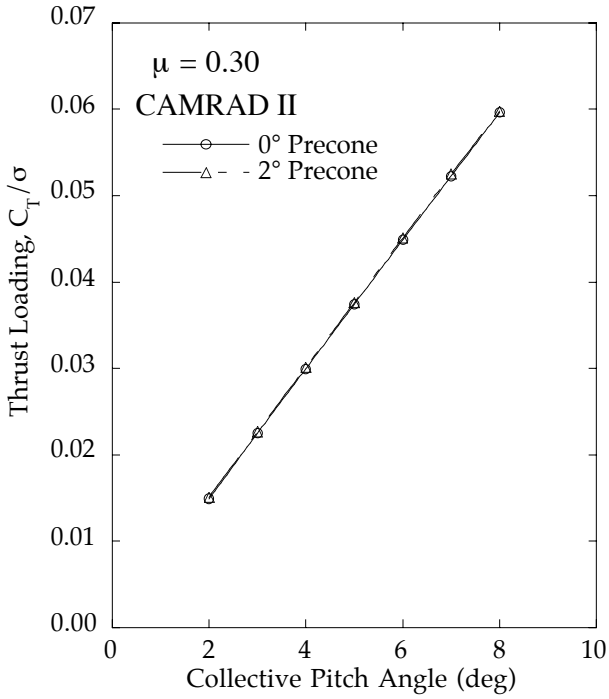

Fig. 27 Swept-tip rotor CAMRAD II calculated thrust loading for two collective sweeps with 0° and 2° precone angles.

highest thrust case to be the 7° collective pitch case for the swept-tip rotor with 0° shaft angle and 0° precone angle. The thrust calculations for the two collective pitch sweeps at an advance ratio of 0.30 are shown in figure 27. Calculation confirms that the maximum thrust of all the forward flight cases is for the 8° collective pitch points shown here.

Conclusions

Regressing lag mode stability data has been obtained in hover and forward flight on two model-scale rotors in two separate test campaigns.

1. Stability data exhibiting very little scatter were obtained in hover for both the straight blade and swept-tip rotors over a range of collective pitch angles.

2. In hover, the measured straight blade rotor damping is substantially higher than the swept-tip rotor over the entire range of collective pitch angles tested.

3. In forward flight, stability data exhibiting very little scatter were obtained over a range of advance ratios, shaft tilts and collective pitch

angles for both the straight blade and swept-tip rotors.

4. For comparable conditions, the change in damping measured on the swept-tip rotor with advance ratio and collective pitch were substantially less than observed on the straight blade rotor.

The CAMRAD II analysis was used to calculate the regressing lag mode damping for both rotors in hover and in forward flight.

1. In hover the predicted lag damping shows very good to excellent agreement with the measurements. The substantial differences in the damping observed between the two rotors are correctly predicted by the analysis.

2. In forward flight the analysis provides fair to very good correlation with the measured lag damping for both rotors. The predictions degrade substantially at the higher thrust levels where the damping is overpredicted.

3. The substantial differences in the lag damping observed for the two rotors in forward flight are also observed in the analytical predictions.

Acknowledgments

The authors extend their appreciation to NASA Ames Research Center Engineering, Machine Shop, Model Shop and Engineering Test Lab for their work on these models. We are indebted to Jon Lautenschlager for his help with instrumentation during critical times, including the week between Christmas and New Years, 1998. And, it must be stated here that these tests could not have been completed without the dedication, hard work, and smarts of Brian Chan, Steve Chan, Joel Gunter, and Dave Pfluger who formed the core experimental test team.

Finally, the guidance of Wayne Johnson with the use of CAMRAD II is greatly appreciated. The quantity and quality of the calculations shown here were made possible with his help.

References

[1] Ormiston, R.A. and Bousman, W.G., "A Theoretical and Experimental Investigation of Flap-Lag Stability of Hingeless Helicopter Rotor Blades," NASA TM X-62-179, August 1972.

[2] Ormiston, R.A. and Bousman, W.G., "A Study of Stall Induced Flap-Lag Instability of Hingeless Rotors, "*Journal of the American Helicopter Society*, Vol. 29, No. 1, January 1975, pp. 20-30.

[3] Bousman, W.G., Sharpe, D.L. and Ormiston, R.A., "An Experimental Study of Techniques for Increasing the Lead-Lag Damping of Soft Inplane Hingeless Rotors," Preprint No. 1035, Proceedings of the American Helicopter Society 32nd National Forum, Washington, D.C., May 1976.

[4] Sharpe, D. L., "An Experimental Investigation of the Flap-Lag-Torsion Aeroelastic Stability of a Small-Scale Hingeless Helicopter Rotor in Hover," NASA TP 2546, AVSCOM TR 85-A-9, 1986.

[5] Bousman, W.G., "The Effects of Structural Flap-Lag and Pitch-Lag Coupling on Soft Inplane Hingeless Rotor Stability in Hover," NASA TP 3002, AVSCOM TR 89-A-002, 1990.

[6] Weller, W.H., "Relative Aeromechanical Stability Characteristics for Hingeless and Bearingless Rotors," *Journal of the American Helicopter Society*, Vol. 35, No. 3, July 1990, pp. 68-77.

[7] Dawson, S., "An Experimental Investigation of the Stability of a Bearingless Model Rotor in Hover," *Journal of the American Helicopter Society*, Vol. 28, No. 4, October 1983, pp. 29-34.

[8] Weller, W.H. and Peterson, R.L., "Inplane Stability Characteristics for an Advanced Bearingless Main Rotor Model," *Journal of the American Helicopter Society*, Vol. 29, No. 3, July 1984, pp. 45-53.

[9] McNulty, M.J., "Flap-Lag Stability Data for a Small-Scale Isolated Hingeless Rotor in Forward Flight," NASA TM 102189, USAAVSCOM TR 89-A-003, April 1989.

[10] Maier, T.H., Sharpe, D.L. and Lim, J.W., "Fundamental Investigation of Hingeless Rotor Aeroelastic Stability, Test Data and Correlation Proceedings of the American Helicopter Society 51st Annual Forum, Fort Worth, TX, May 1995.

[11] Subramanian, S., Gaonkar, G. H. and Maier, T.H., "A Theoretical and Experimental Investigation of Hingeless-Rotor Stability in Trimmed Flight," Proceedings of the 23rd European Rotorcraft Forum, Dresden, Germany, September 1997.

[12] Johnson, W., "CAMRAD II, Comprehensive Analytical Model of Rotorcraft Aerodynamics and Dynamics," Johnson Aeronautics, Palo Alto, CA, 1992-1997.

[13] Hohenemser, K.H. and Yin, S.-K., "Some Applications of the Method of Multiblade Coordinates," *Journal of the American Helicopter Society*, Vol. 17, No. 3, July 1972, pp. 3-12.

[14] Hammond, C.E. and Doggett, R.V., Jr., "Determination of Subcritical Damping by Moving-Block/Randomdec Application," NASA Symposium on Flutter Testing Techniques, NASA SP-415, October 1975, pp. 59-76.

[15] Bousman, W.G. and Winkler, D.J., "Application of the Moving-Block Analysis," Proceedings, AIAA/ASME/ASCE/AHS 22nd Structures, Structural Dynamics, and Materials Conference, Atlanta, Georgia, April 1981, pp. 755-763.